

DESY 94-170
September 1994

CP Violation and Strong Phases from Penguins in $\mathbf{B}^\pm \rightarrow \mathbf{PP}$ and $\mathbf{B}^\pm \rightarrow \mathbf{VP}$ Decays

G. Kramer^a, W. F. Palmer^{b1}, H. Simma^c

^aII. Institut für Theoretische Physik²
der Universität Hamburg,
D-22761 Hamburg, Germany

^bDepartment of Physics, The Ohio State University,
Columbus, Ohio 43210, USA

^cDeutsches Elektronen Synchrotron DESY
D-22603 Hamburg, Germany

Abstract

We calculate direct CP-violating rate asymmetries in charged $B \rightarrow PP$ and $B \rightarrow VP$ decays arising from the interference of amplitudes with different strong and CKM phases. The perturbative strong phases develop at order α_s from absorptive parts of one-loop matrix elements of the next-to-leading logarithm corrected effective Hamiltonian. CPT constraints are maintained. Based on this model, we find that partial rate asymmetries between charge conjugate B^\pm decays can be as high as 20% for certain channels with branching ratios in the 10^{-6} range. Because the $c\bar{c}$ threshold lies so close to the physical momentum scale, the asymmetries depend sensitively on the model assumptions used to evaluate the imaginary parts of the matrix elements, in particular, on the internal momentum transfer. The charge asymmetries of partial rates would provide unambiguous evidence for direct CP violation.

¹Supported in part by the US Department of Energy under contract DOE/ER/01545-605.

²Supported by Bundesministerium für Forschung und Technologie, 05 6 HH 93P(5), Bonn, Germany and EEC Program "Human Capital and Mobility" Network "Physics at High Energy Colliders" CHRX-CT93-0357 (DG 12 COMA)

1 Introduction

So far CP violation [1] has been detected only in processes related to $K^0 - \bar{K}^0$ mixing [2] but considerable efforts are being made to investigate it in B decays. While the most promising proposal for observing CP violation in the B system involves the mixing between neutral B mesons [3], the particular interest in decays of charged B mesons lies in their possibilities for establishing the detailed nature of CP violation. Since charged B mesons can not mix, a measurement of a CP violating observable in these decays would be a clear sign for *direct* CP violation, which has possibly been found in K decays where the measurements of ϵ'/ϵ now seem to favour a non-zero value [4] which is consistent with expectations from the standard model and a top quark mass around 150 GeV [5].

In non-leptonic charged B decays two main categories of direct CP-violating observables can be investigated: First, rate asymmetries [6, 7],

$$a_{CP} = \frac{\Gamma(B^- \rightarrow f) - \Gamma(B^+ \rightarrow \bar{f})}{\Gamma(B^- \rightarrow f) + \Gamma(B^+ \rightarrow \bar{f})}, \quad (1)$$

and second, azimuthal angular correlations [8, 9]. The latter involve the decay of the B meson into two vector particles $B \rightarrow V_1 V_2$ with subsequent decays of V_1 and V_2 [8, 9]. By analyzing the azimuthal dependence of the vector meson decay products one can then isolate CP odd quantities. The advantage of this method is that the CP violating terms occur even when there are no strong phase differences between the interfering weak amplitudes. On the other hand the azimuthal correlations can also be present when the CP-violating weak phase differences vanish. By measuring their coefficients in charge conjugate B^\pm decays one has the possibility to disentangle the effects of strong and weak phases [9, 10].

The rate asymmetries occur even for final states with spinless particles but require both weak *and* strong phase differences in interfering amplitudes. The weak phase differences arise from the superposition of amplitudes from various penguin diagrams and the usual W-exchange (if contributing). It is clear that a significant contribution of penguin diagrams, and hence of the CKM [11] phase differences, is an exceptional case and requires either the absence or a strong CKM suppression of the tree contributions (as e.g. in charmless $b \rightarrow s$ transitions). The strong phase is generated by final state interactions. At the quark level the strong interaction effects can be modeled perturbatively, following Bander, Silverman and Soni [6], by the absorptive part of penguin diagrams. There may be additional final state interaction effects at the non-perturbative hadronic level (soft final state interactions). These are very difficult to estimate, but since the mass of the B is far above the usual resonance region, we expect these phase shifts to be small.

The rate asymmetries for exclusive two-body decays into pseudoscalars are usually estimated using either the model of Bauer, Stech and Wirbel [12] (BSW) based on wave functions in the infinite momentum frame, or the perturbative methods developed by Brodsky et al. [13]. The rate asymmetries a_{CP} can be quite large (of the order $a_{CP} \sim 0.1$) for some of the final states. However, the corresponding branching fractions of these decays are quite small, ranging from 10^{-6} (estimates with the BSW model [12]) to 10^{-7} (estimates with the Brodsky-Lepage model [13, 14, 15]). The number

of B-mesons required to resolve the CP asymmetry experimentally (proportional to $(a_{CP}^2 \times BR)^{-1}$) is therefore at least of the order of 10^8 .

Angular correlations and rate asymmetries for $B \rightarrow VV$ have been investigated in some detail in our previous work [10]. There we considered all possible decay channels of charged B mesons into two vector particle final states which are induced either by $b \rightarrow s$ or $b \rightarrow d$ transitions. We found appreciable rate asymmetries for the transitions $B^- \rightarrow K^{*-} + \omega$, $B^- \rightarrow K^{*-} + \rho^0$, $B^- \rightarrow K^{*-} + K^{*0}$ and $B^- \rightarrow \rho^- + \omega$. For these decays the predicted rates are necessarily small but large enough to be seen in upcoming B factories. These encouraging results have lead us to consider the simpler decay channels of charged B 's into two pseudoscalars (PP) and into one vector plus one pseudoscalar particle (VP) within the same framework as in our recent work for the two vector final state [10]. In $B \rightarrow PP$ and $B \rightarrow VP$ only one helicity amplitude contributes and thus no angular correlation coefficients are at our disposal for detecting direct CP violation. On the other hand rate asymmetries might be easier to measure.

In order to systematically take into account the $O(\alpha_s)$ penguin matrix elements, we base our treatment on the next-to-leading logarithmic short distance corrections evaluated by Buras et al. [16]. We include also some pure penguin modes and give estimates of their branching ratios. In this part there is overlap with other work which we will mention later when we present our results. Briefly, because we have a more complete treatment of the one-loop matrix element, including all the CP constraints of [7, 17] and because we have included all $O(\alpha_s)$ penguins (including so-called 'hairpin' diagrams and pseudoscalar diagrams) our results are more complete than earlier work.

The remainder of this paper is organized as follows. In Sect. 2 we describe the effective weak Hamiltonian and the evaluation of the hadronic matrix elements. The final results for the branching ratios and rate differences are discussed in Sect. 3. A table of formulae for the various decay modes can be found in the appendix.

2 The effective Hamiltonian

In the next two subsections we follow closely our earlier work on $B \rightarrow VV$ decays [10]. To make the paper self-contained we shall repeat some information already given in [10]. In subsection 2.3 we describe the evaluation of the hadronic matrix elements which are relevant for PP and VP final states.

2.1 Short distance QCD corrections

For calculations of CP-violating observables it is most convenient to exploit the unitarity of the CKM matrix and split the effective weak Hamiltonian into two pieces, one proportional to $v_u \equiv V_{ub}V_{us}^*$ (or $V_{ub}V_{ud}^*$ in the case of $b \rightarrow d$ transitions) and the other one proportional to $v_c \equiv V_{cb}V_{cs}^*$ (or $V_{cb}V_{cd}^*$ correspondingly),

$$\mathcal{H}_{\text{eff}} = 4 \frac{G_F}{\sqrt{2}} \left(v_u \mathcal{H}_{\text{eff}}^{(u)} + v_c \mathcal{H}_{\text{eff}}^{(c)} \right). \quad (2)$$

The two terms ($q = u, c$)

$$\mathcal{H}_{\text{eff}}^{(q)} = \sum_i c_i(\mu) \cdot O_i^{(q)} , \quad (3)$$

differ only by the quark content of the local operators, and for our purposes it is sufficient to consider only the following four-quark operators:

$$\begin{aligned} O_1^{(q)} &= \bar{s}_\alpha \gamma^\mu L q_\beta \cdot \bar{q}_\beta \gamma_\mu L b_\alpha , & O_2^{(q)} &= \bar{s}_\alpha \gamma^\mu L q_\alpha \cdot \bar{q}_\beta \gamma_\mu L b_\beta , \\ O_3 &= \bar{s}_\alpha \gamma^\mu L b_\alpha \cdot \sum_{q'} \bar{q}'_\beta \gamma_\mu L q'_\beta , & O_4 &= \bar{s}_\alpha \gamma^\mu L b_\beta \cdot \sum_{q'} \bar{q}'_\beta \gamma_\mu L q'_\alpha , \\ O_5 &= \bar{s}_\alpha \gamma^\mu L b_\alpha \cdot \sum_{q'} \bar{q}'_\beta \gamma_\mu R q'_\beta , & O_6 &= \bar{s}_\alpha \gamma^\mu L b_\beta \cdot \sum_{q'} \bar{q}'_\beta \gamma_\mu R q'_\alpha . \end{aligned} \quad (4)$$

where L and R are the left- and right-handed projection operators. The operators O_3, \dots, O_6 arise from (QCD) penguin diagrams which contribute at order α_s to the initial values of the coefficients at $\mu \approx M_W$ [16], or through operator mixing during the renormalization group summation of short distance QCD corrections [18]. The usual tree-level W -exchange corresponds to O_2 (with $c_2(M_W) = 1 + O(\alpha_s)$). The renormalization group evolution from $\mu \approx M_W$ to $\mu \approx m_b$ has been evaluated in next-to-leading logarithmic (NLL) precision by Buras et al. [16]. These authors also demonstrated how the $O(\alpha_s)$ renormalization scheme dependence can be isolated in terms of a matrix \mathbf{r}_{ij} by writing

$$c_j(\mu) = \sum_i \bar{c}_i(\mu) \left[\delta_{ij} - \frac{\alpha_s(\mu)}{4\pi} \mathbf{r}_{ij} \right] , \quad (5)$$

where the coefficients \bar{c}_j are scheme independent at this order. The numerical values for $\Lambda_{\overline{MS}}^{(4)} = 350$ MeV (which is in accord with $\Lambda_{\overline{MS}}^{(5)} = 240 \pm 90$ MeV from the compilation of G. Altarelli [19]), $m_t = 150$ GeV and $\mu = m_b = 4.8$ GeV are [16]

$$\begin{aligned} \bar{c}_1 &= -0.324 , & \bar{c}_2 &= 1.151 , \\ \bar{c}_3 &= 0.017 , & \bar{c}_4 &= -0.038 , \\ \bar{c}_5 &= 0.011 , & \bar{c}_6 &= -0.047 . \end{aligned} \quad (6)$$

Contributions from the color magnetic moment operator will always be neglected in the following, because already its tree level matrix elements are suppressed by a factor $\alpha_s/4\pi$ and it cannot provide interesting absorptive parts in the decays considered here.

2.2 Quark-level matrix elements

Working consistently at NLL precision, the matrix elements of \mathcal{H}_{eff} are to be treated at the one-loop level in order to cancel the scheme dependence from the renormalization group evolution. The one-loop matrix elements can be rewritten in terms of the tree-level matrix elements of the effective operators:

$$\langle sq' \bar{q}' | \mathcal{H}_{\text{eff}}^{(q)} | b \rangle = \sum_{i,j} c_i(\mu) \left[\delta_{ij} + \frac{\alpha_s(\mu)}{4\pi} \mathbf{m}_{ij}(\mu, \dots) \right] \langle sq' \bar{q}' | O_j^{(q)} | b \rangle^{\text{tree}} . \quad (7)$$

The functions \mathbf{m}_{ij} are determined by the corresponding renormalized one-loop diagrams and depend in general on the scale μ , on the quark masses and momenta, *and* on the

renormalization scheme. The various one-loop diagrams can be grouped into two classes: *vertex-corrections*, where a gluon connects two of the outgoing quark lines (fig. 1a), and *penguin* diagrams, where a quark-antiquark line closes a loop and emits a gluon, which itself decays finally into a quark-antiquark pair (fig. 1b).

When expressing the rhs of (7) in terms of the renormalization scheme independent coefficients \bar{c}_i , the effective coefficients multiplying the matrix elements $\langle sq'\bar{q}'|O_j^{(q)}|b\rangle^{\text{tree}}$ become

$$c_j^{\text{eff}} \equiv \bar{c}_j + \frac{\alpha_s}{4\pi} \sum_i \bar{c}_i \cdot (\mathbf{m}_{ij} - \mathbf{r}_{ij}) . \quad (8)$$

The renormalization scheme dependence, which is present in \mathbf{m}_{ij} and \mathbf{r}_{ij} , explicitly cancels in the combination $\mathbf{m}_{ij} - \mathbf{r}_{ij}$ [16].

The effective coefficients $c_{1,2}^{\text{eff}}$ receive contributions only from *vertex-correction* diagrams, which will not be included in the following (see discussion at the end of Section 2.3). For a general $SU(N)$ color group the remaining effective coefficients can be brought into the following form

$$\begin{aligned} c_3^{\text{eff}} &= \bar{c}_3 - \frac{1}{2N} \frac{\alpha_s}{4\pi} (c_t + c_p) + \dots \\ c_4^{\text{eff}} &= \bar{c}_4 + \frac{1}{2} \frac{\alpha_s}{4\pi} (c_t + c_p) + \dots \\ c_5^{\text{eff}} &= \bar{c}_5 - \frac{1}{2N} \frac{\alpha_s}{4\pi} (c_t + c_p) + \dots \\ c_6^{\text{eff}} &= \bar{c}_6 + \frac{1}{2} \frac{\alpha_s}{4\pi} (c_t + c_p) + \dots , \end{aligned} \quad (9)$$

where we have separated the contributions c_t and c_p from the “tree” operators $O_{1,2}$ and from the penguin operators $O_{3\dots 6}$, respectively. The ellipses denote further contributions from *vertex-correction* diagrams.

In addition to the contributions from penguin diagrams with insertions of the tree operators $O_{1,2}^{(q)}$

$$c_t = \bar{c}_2 \cdot \left[\frac{10}{9} + \frac{2}{3} \ell n \frac{m_q^2}{\mu^2} - \Delta F_1 \left(\frac{k^2}{m_q^2} \right) \right] , \quad (10)$$

where ΔF_1 is defined in [10], we have evaluated the penguin diagrams for the matrix elements of the penguin operators:

$$\begin{aligned} c_p &= \bar{c}_3 \cdot \left[\frac{280}{9} + \frac{2}{3} \ell n \frac{m_s^2}{\mu^2} + \frac{2}{3} \ell n \frac{m_b^2}{\mu^2} - \Delta F_1 \left(\frac{k^2}{m_s^2} \right) - \Delta F_1 \left(\frac{k^2}{m_b^2} \right) \right] \\ &+ (\bar{c}_4 + \bar{c}_6) \cdot \sum_{j=u,d,s,\dots} \left[\frac{10}{9} + \frac{2}{3} \ell n \frac{m_j^2}{\mu^2} - \Delta F_1 \left(\frac{k^2}{m_j^2} \right) \right] , \end{aligned} \quad (11)$$

Note that the coefficients c_i^{eff} depend on k^2 and, as we shall see later, on the $q\bar{q}$ states that are included in the sum over the intermediate states.

2.3 Hadronic matrix elements in the BSW model

To take into account long distance QCD effects which build up the hadronic final states, we follow Bauer, Stech and Wirbel [12]: With the help of the factorization hypothesis

[20] the three-hadron matrix elements are split into vacuum-meson and meson-meson matrix elements of the quark currents entering in O_1, \dots, O_6 . In addition, OZI suppressed form factors and annihilation terms are neglected. In the BSW model, the meson-meson matrix elements of the currents are evaluated by overlap integrals of the corresponding wave functions and the dependence on the momentum transfer (which is equal to the mass of the factorized meson) is modeled by a single-pole ansatz. As a first approximation, this calculational scheme provides a reasonable method for estimating the relative size and phase of the tree and penguin terms that give rise to the CP-violating signals. It is known that the BSW matrix elements do not describe fully the existing experimental information on decays like $B \rightarrow J/\psi + K, J/\psi + K^*$ [21]. But this should not matter too much for the estimates of CP effects presented here.

Compared to the transitions $B \rightarrow VV$ treated in our earlier work [10] the amplitudes for $B \rightarrow PP$ and $B \rightarrow PV$ have a simpler structure because only one helicity state contributes. On the other hand there are additional contributions from the $(V + A)$ penguin operator O_6 : After Fierz reordering and factorization it contributes in terms which involve a matrix element of the quark-density operators between a pseudoscalar meson and the vacuum

$$\langle P_1 M_2 | O_6 | B \rangle = -2 \sum_q \left(\langle P_1 | \bar{q} b_L | 0 \rangle \langle M_2 | \bar{s} q_R | B \rangle + \langle M_2 | \bar{q} b_L | 0 \rangle \langle P_1 | \bar{s} q_R | B \rangle \right). \quad (12)$$

Using the Dirac equation, the matrix elements entering here can be rewritten in terms of those involving usual $(V - A)$ currents,

$$\langle P_1 M_2 | O_6 | B \rangle = R[P_1, M_2] \langle P_1 M_2 | O_4 | B \rangle, \quad (13)$$

with

$$R[P_1, M_2] \equiv \frac{\pm 2 M_{P_1}^2}{(m_{q1} + m_{\bar{q}1})(m_b \mp m_{q2})}. \quad (14)$$

Here, m_{q1} ($m_{\bar{q}1}$) and m_{q2} are the current masses of the (anti-)quark in the mesons P_1 and M_2 , respectively, and the the upper (lower) sign is for the PP (PV) final state. We use the quark masses $m_u = m_d = 10$ MeV, $m_s = 200$ MeV, $m_c = 1.5$ GeV and $m_b = 4.8$ GeV.

Finally, one arrives at the form

$$\begin{aligned} \langle P_1 M_2 | \mathcal{H}_{\text{eff}}^{(q)} | B \rangle &= Z_1^{(q)} \langle P_1 | j^\mu | 0 \rangle \langle M_2 | j_\mu | B \rangle \\ &+ Z_2^{(q)} \langle M_2 | j'^\mu | 0 \rangle \langle P_1 | j'_\mu | B \rangle, \end{aligned} \quad (15)$$

where j_μ and j'_μ are the corresponding (neutral or charged) $V - A$ currents. The factorization coefficients $Z_1^{(q)}$ and $Z_2^{(q)}$ are listed in the appendix. In terms of the form factors $F_{0,1}$ and A_0 for the current matrix elements defined by BSW [12], this yields

$$\langle P_1 P_2 | \mathcal{H}_{\text{eff}}^{(q)} | B \rangle = Z_1^{(q)} (M_B^2 - M_2^2) f_{P_1} F_0(M_1^2) + Z_2^{(q)} (M_B^2 - M_1^2) f_{P_2} F_0(M_2^2), \quad (16)$$

$$\langle P_1 V_2 | \mathcal{H}_{\text{eff}}^{(q)} | B \rangle = \lambda^{\frac{1}{2}} (M_B^2, M_P^2, M_V^2) \left(Z_1^{(q)} f_P A_0(M_P^2) + Z_2^{(q)} f_V F_1(M_V^2) \right). \quad (17)$$

M_B is the mass of the decaying B meson and f_P (f_V) are the decay constants of the pseudoscalar (vector) mesons in the final state.

Concerning how $1/N$ terms are treated in the coefficients (see (9) and (21)), it is well known [22] that this model has problems accounting for the decays with branching ratios which are proportional to the combination $\bar{c}_1 + \bar{c}_2/N$. This is due to the rather small absolute value of this particular combination when using the short-distance QCD corrected coefficients³. An analogous effect is also known in nonleptonic D decays [12], and several authors advocated a modified procedure to evaluate the factorized amplitudes [12, 24]: There, only terms which are dominant in the $1/N$ expansion are taken into account. Recently there has been much discussion in the literature concerning these issues. Some authors have argued that QCD sum rules validate this procedure [25]. We also choose this leading $1/N$ approximation in evaluating the matrix elements of the weak Hamiltonian and we use the QCD corrected coefficient functions \bar{c}_i given above.

The strong phase shifts are generated in our model only by the absorptive parts (hard final state interactions) of the quark-level matrix elements of the effective Hamiltonian. Of course, when factorizing the hadronic matrix elements, all information on the crucial value of the momentum transfer k^2 of the gluon in the penguin diagram (fig. 1b) is lost. While there has been an attempt [14] to model a more realistic momentum distribution by taking into account the exchange of a hard gluon, we will use here for simplicity only a fixed value of k^2 . From simple two body kinematics [26] or from the investigations in ref. [14] one expects k^2 to be typically in the range

$$\frac{m_b^2}{4} \lesssim k^2 \lesssim \frac{m_b^2}{2}. \quad (18)$$

The results we shall present are sensitive to k^2 in this range because the $c\bar{c}$ threshold lies between these limits. Arguments have been made that the lower limit is a more appropriate choice [17]. In this work we follow [10] and choose the upper limit for our numerical presentation in the tables. However, we have studied the asymmetries as a function of k^2 and will show the results later in Fig. 2-4.

While the next-to-leading logarithmic precision of the effective Hamiltonian allows one to consistently calculate all amplitudes at order α_s and to include all one-loop matrix elements, some care is necessary when evaluating CP-violating asymmetries of the decay rates. In particular, one should make sure that the rate asymmetries for sufficiently inclusive channels remain consistent with CPT constraints in certain mass limits [7]. This issue has been discussed in some detail in [10] and we shall follow a similar procedure of neglecting absorptive parts from flavor diagonal rescattering.

We refined here the approximation of ref. [10] by dropping only those fractions of the imaginary parts of $\Delta F_1(k^2/m_q^2)$ in (10) and (11) which correspond to the projection of the intermediate quark state containing a $q\bar{q}$ -pair onto the final state. Moreover, no absorptive parts of vertex correction diagrams are included in our calculations, because they are always flavour diagonal. Of course, this approach may overestimate the CPT cancellation of the absorptive phases. We have explicitly checked for all decay channels that taking into account the full imaginary parts of the penguin-like matrix elements (10) and (11) — including flavour-diagonal contributions — does not significantly change

³An interesting analysis of the value of $c_1 + c_2/N$ has recently been presented in ref. [23] pointing out the renormalization dependence of the QCD short distance corrections

our results. For the most sensitive cases $B \rightarrow \pi^- \eta'$ and $B \rightarrow \rho^- \eta'$ the inclusion of all intermediate flavours would shift the asymmetries by at most -10% , which is in these cases still less than the uncertainties from the value of k^2 .

As a result of our procedure, the factorization coefficients $Z_{1,2}^{(q)}$ depend not only on whether the basic tree level operator is of the $u\bar{u}$ or $c\bar{c}$ type, and on the effective value of k^2 , but also on the quark content ($u\bar{u}, d\bar{d}, s\bar{s}, c\bar{c}$) contributing in the one-loop penguin matrix elements. As in [10] we do not explicitly drop higher order terms which arise, for instance, through interferences among (real and imaginary parts of) the order α_s matrix elements. However, such terms can not introduce the above mentioned inconsistencies with CPT because the flavour-diagonal absorptive parts are discarded.

3 Results and Discussion

For a numerical analysis of the decay parameters and their CP-violating effects within our model, we need to specify the CKM matrix elements and the current form factors. It is well known [27] that fits for the parameters ⁴

$$\begin{aligned}\rho &= \cos\delta_{13} s_{13}/(s_{12}s_{23}) \\ \eta &= \sin\delta_{13} s_{13}/(s_{12}s_{23})\end{aligned}\tag{19}$$

of the CKM matrix depend critically on the value of the B -meson decay constant f_B . The solution for lower f_B values leads to a negative ρ while higher f_B values render ρ positive.

We have calculated our results for the two solutions, with the values

$$\begin{aligned}\rho = 0.32, \quad \eta = 0.31, \quad (f_B = 250 \text{ MeV}, m_t = 135 \pm 27 \text{ GeV}) \\ \rho = -0.41, \quad \eta = 0.18, \quad (f_B = 125 \text{ MeV}, m_t = 172 \pm 15 \text{ GeV})\end{aligned}$$

from the analysis by Schmidtler and Schubert[27]. A more recent analysis by Ali and London [29] based on the latest information on V_{ub} yields similar results.

The results for the modes which get contributions from tree and penguin diagrams are collected in Tab. 1, 2, 3 and 4. They are obtained with $k^2 = m_b^2/2$ as in our earlier work [10] and for the two CKM parametrizations which we call the $\rho > 0$ and $\rho < 0$ solution, in the following discussion. The results for $B \rightarrow PP$ are given in Tab. 1 ($b \rightarrow s$ transitions) and Tab. 2 ($b \rightarrow d$ transitions). $B \rightarrow PV$ results are given in Tab. 3 ($b \rightarrow s$ transitions) and Tab. 4 ($b \rightarrow d$ transitions). The pattern of branching ratios of the various channels is rather similar for $B \rightarrow PP$, $B \rightarrow PV$ and $B \rightarrow VV$ [10]. Compared to $B \rightarrow VV$ decays considered in [10] the branching ratios are similar but the asymmetries are somewhat smaller. Nevertheless there are some interesting cases with large enough branching ratios and asymmetries to be measurable in currently planned machines. Some differences between the pattern for $B \rightarrow PP$ and VP and that for $B \rightarrow VV$ are due to the contribution of the operator O_6 (see (13)).

If we look at specific decay channels the most interesting cases in Tab. 1 are the decays $B^- \rightarrow K^- + \eta'$ and $B^- \rightarrow K^- + \pi^0$. The branching ratios are of the order

⁴ These coincide with the parameters ρ and η of the Wolfenstein representation for small angles [28].

of 10^{-5} and the asymmetries in the several percent range. For $\rho > 0$ they are larger than for $\rho < 0$ whereas the branching ratios show the opposite pattern. The channel $B^- \rightarrow \pi^- + \overline{K^0}$ is a pure penguin transition with a moderately large branching ratio but a small asymmetry. In Tab. 2 $B^- \rightarrow \pi^- + \pi^0$ has no asymmetry since the penguins cancel due to isospin symmetry. Interesting cases are $B^- \rightarrow \pi^- + \eta$ and $B^- \rightarrow \pi^- + \eta'$ with branching ratios of the order of 10^{-5} and asymmetries of several percent. It is interesting to note that $B^- \rightarrow D^- + D^0$ has a substantial rate as well as an asymmetry of the order of 2%, independent of whether ρ is positive or negative. The last channel, $B^- \rightarrow K^- + K^0$ is again a pure penguin transition with large asymmetry for positive ρ but with a small branching ratio.

In Tab. 3 we give the $B \rightarrow PV$ results ($b \rightarrow s$ transitions). The cases with the biggest asymmetries have very small branching ratios ($\approx 10^{-7}$). Interesting decays are $B^- \rightarrow K^{*-} + \eta'$, $B^- \rightarrow K^{*-} + \eta$ and $B^- \rightarrow K^{*-} + \pi^0$. The three last pairs of decays at the bottom of Tab. 3 are again pure penguin modes which have reasonable branching ratios but small asymmetries.

Tab. 4 contains the results for $B \rightarrow PV$ ($b \rightarrow d$ transitions). The last three pairs of decays in this table are again pure penguin modes. The transition $B^- \rightarrow \pi^- + \phi$ has zero asymmetry since no (absorptive) penguin-like matrix elements are present in the contributing factorization due to its color structure. The other pure penguin modes show appreciable asymmetries for the positive ρ solution. Their branching ratios are small, however. Concerning the other decays, the channel $B^- \rightarrow \rho^- + \eta'$ stands out with a branching ratio of 10^{-5} and an asymmetry of 14% for positive ρ and a branching ratio of 6×10^{-5} with an asymmetry of 1.2% for the negative ρ solution. Other interesting cases are $B^- \rightarrow \rho^- + \eta$, $B^- \rightarrow \rho^- + \pi^0$, $B^- \rightarrow \pi^- + \omega$ and $B^- \rightarrow \pi^- + \rho^0$ with significant asymmetries. For $\rho < 0$ the asymmetries are usually smaller than for $\rho > 0$ but then the branching ratios are larger.

Of course, these results can not be considered definitive since we had to make a series of model assumptions namely factorization, BSW matrix elements and the modelling of the absorptive contributions in terms of penguin matrix elements. Factorization is receiving increasing experimental support [21] and also most of the BSW matrix elements have been tested experimentally in unsuppressed decays [22]. We are aware of the colour suppression problem concerning the sign of $c_1 + c_2/N$ [21, 22]. But we prefer to stay in line with the conventional QCD framework together with factorization and the limit $N \rightarrow \infty$.

As in the case of $B \rightarrow VV$ decays, the inclusion of $1/N$ terms would decrease the branching ratios for each of the channels involving a $c\bar{c}$ -meson by about a factor of 25. Other channels which are drastically effected by including $1/N$ terms are $B^- \rightarrow \pi^- \Phi$, and $B^- \rightarrow K^- \omega$, where the branching ratios are decreased by four orders of magnitude and a factor of about 20, respectively. In all other channels, the effect of treating the $1/N$ terms amounts to a change by less than a factor of two for the prediction of the branching ratios or asymmetries (which generally change in the opposite direction).

A major simplification in our model is that we evaluated the matrix elements at fixed $k^2 = m_b^2/2$. This determines the imaginary parts of the penguin diagrams. In a more elaborate treatment the effective k^2 would be determined by the dynamics. Here we relied on the work of [26] and [14] yielding a range of values given in (18) of

which we have chosen the upper limit. To get an idea how the asymmetries change with k^2 we have calculated the asymmetries as a function of k^2/m_b^2 . The results are shown in Fig. 2, 3 and 4. Starting at zero for $k^2 = 0$ the asymmetries vary quite appreciably with k^2 (depending on the thresholds appearing in the matrix elements), even when k^2 is restricted to the interval (18). Only for the transitions $B^- \rightarrow D^- + D^0$ and $B^- \rightarrow D^- + D^{0*}$ the asymmetry is essentially independent of k^2 . It is clear that the results presented in the tables in most cases are sensitive to k^2 . A more detailed investigation, channel by channel, is needed to get a better estimate of the effective value of k^2 , for example, using the approach of Brodsky et al. [13] which includes extra gluon exchange or the model of Greub and Wyler [30] using wave functions.

In Tab. 1, 2, 3 and 4 we have given also results for some Cabibbo allowed channels $B^- \rightarrow K^- + \eta_c$, $D_s^- + D^0$, $D^- + D^0$, $K^- + J/\psi$, $D^0 + D_s^{*-}$, $K^{*-} + \eta_c$, $D^{*0} + D_s^-$, $D^0 + D^{*-}$ and $D^{*0} + D^-$ for completeness. These results can be used for testing some of our model assumptions. In these cases the asymmetries are not significant except perhaps for $B^- \rightarrow D^0 + D^{*-}$ and $B^- \rightarrow D^{*0} + D^-$. The channels with two charmed mesons in the final state could also be calculated in the frame work of the heavy quark effective theory which would be more rigorous than using BSW matrix elements. However, it would give similar branching ratios [31] and asymmetries (assuming factorization and a fixed value of k^2).

We mention that some of the modes have been calculated by other authors using a similar approach. First there is work on pure penguin modes [15, 32, 33] and also some work on modes where penguins interfere with tree diagrams [34]. Our results are in qualitative agreement with these efforts. The work presented here is more elaborate, because it includes NLO corrections in the QCD coefficients for the tree diagrams and in the penguin contributions which were not taken into account in [34]. Therefore it is not too meaningful to make detailed comparisons with this work. The k^2 dependence of asymmetries for some selected channels has been studied also [35, 34, 33, 15, 32] with similar results to ours.

The branching ratios we have presented in Tab. 1-4 are well within experimental limits. However there are three channels where the most recent limits [36] come within factors of 2-3 of our predictions: $K^0\pi^+$, $K^{*0}\pi^+$, $K^+\pi^0$. It is therefore clear that the next generation of experiments can provide stringent tests of our model.

Acknowledgement

W. F. P. thanks the Desy Theory Group for its kind hospitality and the North Atlantic Treaty Organization for a Travel Grant. He is also grateful for helpful conversations with K. Honscheid.

4 Appendix

The factorization coefficients $Z_{1,2}^{(q)}$ defined in (15) are listed in Tab. 5 for $B \rightarrow PP$ channels. For the case of $B \rightarrow PV$ decays the factorization coefficients are obtained by replacing one of the pseudoscalars by a vector meson with the corresponding flavour

content, and by setting $R[M, P] = 0$ if M is a vector meson.

In Tab. 5 we refer to the unphysical states

$$\eta_u \equiv \frac{1}{\sqrt{2}}(u\bar{u} + d\bar{d}), \quad \eta_s \equiv s\bar{s}, \quad (20)$$

which are related to the physical η -mesons by taking into account corresponding mixing angles. The table covers both cases, $q = u$ and $q = c$, of (15); by use of the Kronecker delta the contributions from the operators $O_{1,2}$ are to be dropped when tree contributions are absent for the given CKM prefactor, see (2). Colour suppressed terms may readily be included in the coefficients

$$a_i \equiv c_i^{\text{eff}} + \frac{1}{N}c_j^{\text{eff}} \quad (21)$$

where $\{i, j\}$ is any of the pairs $\{1, 2\}$, $\{3, 4\}$, or $\{5, 6\}$. In Tab. 5 we have adopted the convention of including factors of $\sqrt{2}$ associated with a neutral meson P_2 . They arise either from current matrix elements between P_2 and B (left column), or from the definition of the decay constants for P_2 (right column). Care should be taken with the latter since these factors are sometimes absorbed into the decay constants (e.g. as tabulated in [12]).

References

- [1] *CP Violation*, Editor C. Jarlskog, Advanced Series on Directions in High Energy Physics, Vol. 3, World Scientific, Singapore, New Jersey, London, Hong Kong, 1989.
- [2] J. H. Christenson, J. W. Cronin, V. L. Fitch, R. Turlay, Phys. Rev. Lett. 13 (1964) 138.
- [3] I.I. Bigi et al. in *CP Violation*, Editor C. Jarlskog, Advanced Series on Directions in High Energy Physics, Vol. 3, World Scientific, Singapore, New Jersey, London, Hong Kong, 1989 and the earlier literature quoted there.
- [4] G. D. Barr et al., NA31 Collaboration, Phys. Lett. B317 (1993) 233; L. K. Gibbons et al., E731 Collaboration, Phys. Rev. Lett. 70 (1993) 1203.
- [5] G. Buchalla, A. J. Buras, M. K. Harlander, Nucl. Phys. B349 (1991) 1, A. J. Buras et al., Nucl. Phys. B370 (1992) 69.
- [6] M. Bander, D. Silverman, A. Soni, Phys. Rev. Lett. 43 (1979) 242.
- [7] J. M. Gerard, W. S. Hou, Phys. Rev. Lett 62 (1989) 855, Phys. Rev. D43 (1991) 2909.
- [8] G. Valencia, Phys. Rev. D39 (1989) 3339.
- [9] G. Kramer, W. F. Palmer, Phys. Rev D45 (1992) 132, Phys. Lett. B279 (1992) 181, Phys. Rev. D46 (1992) 2969.
- [10] G. Kramer, W. F. Palmer, H. Simma, DESY report 93-192, December 1993, Nucl. Phys. B (to be published).
- [11] N. Cabibbo, Phys. Rev. Lett. 10 (1963) 531; M. Kobayash, T. Maskawa, Prog. Theor. Phys. 49 (1973) 652.
- [12] M. Bauer, B. Stech, M. Wirbel, Z. Phys. C34 (1987) 103, *ibid* C29 (1985) 637.
- [13] S.J. Brodsky, P. Lepage. Phys. Lett. B87 (1979) 359 and Phys. Rev. D22 (1980) 2157; A. Szczepaniak, E.M. Henley, S.J. Brodsky, Phys. Lett. B243 (1990) 287.
- [14] H. Simma, D. Wyler, Phys. Lett. B272 (1991) 395.
- [15] R. Fleischer, Z. Phys. C58 (1993) 483.
- [16] A. Buras et al., Nucl. Phys. B370 (1992) 69.
- [17] J. M. Gerard, W.S. Hou, Phys. Rev. D43 (1991) 2909; H. Simma, G. Eilam, D. Wyler, Nucl. Phys. B352 (1991) 367.
- [18] M.A. Shifman, A.I. Vainshtein, V.I. Zakharov, Nucl. Phys. B120 (1977) 316, Sov. Phys. JETP 45 (1977) 670, F. Gilman, M. Wise, Phys. Rev. D20 (1979) 2392, W. Ponce, Phys. Rev. D23 (1981) 1134.

- [19] G. Altarelli in Proceedings of *QCD 20 Years Later*, edited by P.M. Zerwas and H. A. Kastrup, Aachen, June 9–13, 1992 World Scientific, Singapore, New Jersey, London, Hong Kong, 1993.
- [20] D. Fakirov, B. Stech, Nucl. Phys. B133 (1978) 315, N. Cabibbo, L. Maiani, Phys. Lett. 73B (1978) 418 and earlier references given there.
- [21] M. S. Alam et al., CLEO Collaboration, Phys. Rev. D50 (1994) 43
- [22] H. Albrecht et al., ARGUS Collaboration, Z. Phys. C48 (1990) 543, D. Bortoletto et. al., CLEO Collaboration, Phys. Rev. D45 (1992) 21.
- [23] A. J. Buras, MPI preprint, MPI-PhT/94-60.
- [24] A. J. Buras, J. M. Gerard, R. Rückl, Nucl. Phys. B268 (1986) 16; W. A. Bardeen, A. J. Buras, J.M. Gerard, Phys. Lett. B180 (1980) 133.
- [25] B. Blok, M. Shifman, Sov. Journ. Nucl. Phys. 45 (1987) 135,301,522.
- [26] N.G. Deshpande, J. Trampetic, Phys. Rev. D41 (1990) 2926.
- [27] M. Schmidtler, K. Schubert, Z. Phys. C53 (1992) 347.
- [28] L. Wolfenstein, Phys. Rev. Lett. 51 (1983) 1945.
- [29] A. Ali, D. London in ECFA Workshop on a European *B*-Meson Factory, *B* Physics Working Group Report. Editors R. Aleksan (Saclay) and A. Ali (DESY), ECFA 93/151, DESY 93-053, p. 42-68; A. Ali, D. London, CERN-TH 7248/94, May 1994, Z. Phys. C (to be published).
- [30] C. Greub, D. Wyler, Phys. Lett. B295 (1992) 293.
- [31] G. Kramer, T. Mannel, W. F. Palmer, Z. Phys. C55 (1992) 497.
- [32] R. Fleischer, Z. Phys. C62 (1994) 81.
- [33] D. Du, Z. Xing, preprint, Institute of High Energy Physics, Beijing.
- [34] D. Du, Z. Xing, Phys. Rev. D48 (1993) 4155
- [35] D. Du, Z. Xing, Phys. Lett. B280 (1992) 292
- [36] J. Gronberg et al., CLEO Collaboration, preprint, CLEO CONF 94-3, July 18, 1994.

Figure captions

Fig. 1: Two types of one-loop matrix elements: (a) Vertex corrections, and (b) penguin diagrams. The square box denotes an insertion of one of the four-quark operators O_i of (4).

Fig. 2: Momentum dependence of the asymmetry parameter a_{CP} for $B \rightarrow PP$ transitions and a ρ positive CKM Matrix.

Fig. 3: Momentum dependence of the asymmetry parameter a_{CP} for $B \rightarrow PV$ ($b \rightarrow s$ transitions) and a ρ positive CKM Matrix.

Fig. 4: Momentum dependence of the asymmetry parameter a_{CP} for $B \rightarrow PV$ ($b \rightarrow d$ transitions) and a ρ positive CKM Matrix.

Table captions

Tab. 1: Branching ratios and rate asymmetries for $B \rightarrow PP$ ($b \rightarrow s$ transitions) for a ρ positive and a ρ negative CKM Matrix, and for $k^2 = m_b^2/2$. Values in parentheses correspond to the case without strong phases.

Tab. 2: Branching ratios and rate asymmetries for $B \rightarrow PP$ ($b \rightarrow d$ transitions) for a ρ positive and a ρ negative CKM Matrix, and for $k^2 = m_b^2/2$. Values in parentheses correspond to the case without strong phases.

Tab. 3: Branching ratios and rate asymmetries for $B \rightarrow PV$ ($b \rightarrow s$ transitions) for a ρ positive and a ρ negative CKM Matrix, and for $k^2 = m_b^2/2$. Values in parentheses correspond to the case without strong phases.

Tab. 4: Branching ratios and rate asymmetries for $B \rightarrow PV$ ($b \rightarrow d$ transitions) for a ρ positive and a ρ negative CKM Matrix, and for $k^2 = m_b^2/2$. Values in parentheses correspond to the case without strong phases.

Tab. 5: Factorization coefficients $Z_{1,2}^{(q)}$ for various $B \rightarrow P_1P_2$ decays. The short distance coefficients a_i are defined in (21) and the factor R is given in (14).

Table 1:

$B \rightarrow PP$ ($b \rightarrow s$ transitions)				
Matrix Elements <i>with (without)</i> Strong Phases for $k^2 = m_b^2/2$				
CKM Matrix:	$\rho = 0.32, \eta = 0.31$		$\rho = -0.41, \eta = 0.18$	
Channel	BR	$a_{CP}[\%]$	BR	$a_{CP}[\%]$
$B^- \rightarrow K^- + \eta$	1.4×10^{-6}	-3.2	2.0×10^{-7}	-12.
$B^+ \rightarrow K^+ + \eta$	1.5×10^{-6} (1.4×10^{-6})		2.5×10^{-7} (2.2×10^{-7})	
$B^- \rightarrow K^- + \eta'$	7.8×10^{-6}	5.7	1.0×10^{-5}	2.5
$B^+ \rightarrow K^+ + \eta'$	7.0×10^{-6} (6.6×10^{-6})		9.4×10^{-6} (8.9×10^{-6})	
$B^- \rightarrow K^- + \pi^0$	6.0×10^{-6}	8.1	1.1×10^{-5}	2.3
$B^+ \rightarrow K^+ + \pi^0$	5.1×10^{-6} (5.3×10^{-6})		1.1×10^{-5} (1.1×10^{-5})	
$B^- \rightarrow K^- + \eta_c$	1.9×10^{-3} (1.9×10^{-3})	0.0	1.9×10^{-3} (1.9×10^{-3})	0.0
$B^- \rightarrow D_S^- + D^0$	7.1×10^{-3}	-0.12	7.1×10^{-3}	-0.069
$B^+ \rightarrow D_S^+ + \overline{D^0}$	7.1×10^{-3} (7.1×10^{-3})		7.1×10^{-3} (7.1×10^{-3})	
$B^- \rightarrow \pi^- + \overline{K^0}$	2.0×10^{-5}	0.51	1.9×10^{-5}	0.31
$B^+ \rightarrow \pi^+ + K^0$	2.0×10^{-5} (1.9×10^{-5})		1.9×10^{-5} (1.8×10^{-5})	

Table 2:

$B \rightarrow PP$ ($b \rightarrow d$ transitions)				
Matrix Elements <i>with</i> (<i>without</i>) Strong Phases for $k^2 = m_b^2/2$				
CKM Matrix:	$\rho = 0.32, \eta = 0.31$		$\rho = -0.41, \eta = 0.18$	
Channel	BR	$a_{CP}[\%]$	BR	$a_{CP}[\%]$
$B^- \rightarrow \pi^- + \eta$	6.6×10^{-6}	-13.	2.1×10^{-6}	-21.
$B^+ \rightarrow \pi^+ + \eta$	8.6×10^{-6} (7.5×10^{-6})		3.2×10^{-6} (2.4×10^{-6})	
$B^- \rightarrow \pi^- + \eta'$	1.9×10^{-5}	-12.	3.3×10^{-5}	-4.3
$B^+ \rightarrow \pi^+ + \eta'$	2.5×10^{-5} (2.2×10^{-5})		3.6×10^{-5} (3.3×10^{-5})	
$B^- \rightarrow \pi^- + \pi^0$	5.6×10^{-6} (5.6×10^{-6})	0.0	5.7×10^{-6} (5.7×10^{-6})	0.0
$B^- \rightarrow \pi^- + \eta_c$	8.4×10^{-5} (8.4×10^{-5})	0.0	7.3×10^{-6} (7.3×10^{-6})	0.0
$B^- \rightarrow D^- + D^0$	4.0×10^{-4}	2.2	3.4×10^{-4}	1.5
$B^+ \rightarrow D^+ + \overline{D^0}$	3.8×10^{-4} (3.9×10^{-4})		3.3×10^{-4} (3.4×10^{-4})	
$B^- \rightarrow K^- + K^0$	6.8×10^{-7}	-17.	2.3×10^{-6}	-3.3
$B^+ \rightarrow K^+ + \overline{K^0}$	9.4×10^{-7} (7.8×10^{-7})		2.5×10^{-6} (2.2×10^{-6})	

Table 3:

$B \rightarrow PV$ ($b \rightarrow s$ transitions)				
Matrix Elements <i>with (without)</i> Strong Phases for $k^2 = m_b^2/2$				
CKM Matrix:	$\rho = 0.32, \eta = 0.31$		$\rho = -0.41, \eta = 0.18$	
Channel	BR	$a_{CP}[\%]$	BR	$a_{CP}[\%]$
$B^- \rightarrow K^- + \omega$	7.4×10^{-6}	1.0	4.2×10^{-6}	1.0
$B^+ \rightarrow K^+ + \omega$	7.3×10^{-6} (7.3×10^{-6})		4.1×10^{-6} (4.1×10^{-6})	
$B^- \rightarrow K^- + \rho^0$	2.7×10^{-7}	34.	9.4×10^{-7}	4.4
$B^+ \rightarrow K^+ + \rho^0$	1.4×10^{-7} (1.8×10^{-7})		8.6×10^{-7} (8.8×10^{-7})	
$B^- \rightarrow K^- + J/\psi$	9.0×10^{-4} (9.0×10^{-4})	0.0	9.1×10^{-4} (9.1×10^{-4})	0.0
$B^- \rightarrow D_S^{*-} + D^0$	8.8×10^{-3}	-0.047	8.8×10^{-3}	-0.027
$B^+ \rightarrow D_S^{*+} + \overline{D^0}$	8.8×10^{-3} (8.8×10^{-3})		8.8×10^{-3} (8.8×10^{-3})	
$B^- \rightarrow K^{*-} + \eta$	3.4×10^{-7}	45.	9.9×10^{-7}	6.7
$B^+ \rightarrow K^{*+} + \eta$	1.3×10^{-7} (2.2×10^{-7})		8.7×10^{-7} (9.2×10^{-7})	
$B^- \rightarrow K^{*-} + \eta'$	1.5×10^{-6}	13.	2.5×10^{-7}	64.
$B^+ \rightarrow K^{*+} + \eta'$	1.2×10^{-6} (1.3×10^{-6})		5.7×10^{-8} (9.7×10^{-8})	
$B^- \rightarrow K^{*-} + \pi^0$	3.9×10^{-6}	19.	1.1×10^{-5}	3.4
$B^+ \rightarrow K^{*+} + \pi^0$	2.6×10^{-6} (3.1×10^{-6})		1.0×10^{-5} (1.1×10^{-5})	
$B^- \rightarrow K^{*-} + \eta_c$	5.8×10^{-4} (5.8×10^{-4})	0.0	5.8×10^{-4} (5.8×10^{-4})	0.0
$B^- \rightarrow D_S^- + D^{*0}$	4.0×10^{-3}	-0.013	4.0×10^{-3}	-0.007
$B^+ \rightarrow D_S^+ + \overline{D^{*0}}$	4.0×10^{-3} (4.0×10^{-3})		4.0×10^{-3} (4.0×10^{-3})	
$B^- \rightarrow \pi^- + \overline{K^{*0}}$	1.5×10^{-5}	0.54	1.4×10^{-5}	0.33
$B^+ \rightarrow \pi^+ + K^{*0}$	1.5×10^{-5} (1.4×10^{-5})		1.4×10^{-5} (1.3×10^{-5})	
$B^- \rightarrow K^- + \phi$	5.8×10^{-6}	1.2	5.5×10^{-6}	0.75
$B^+ \rightarrow K^+ + \phi$	5.7×10^{-6} (4.5×10^{-6})		5.4×10^{-6} (4.3×10^{-6})	
$B^- \rightarrow \rho^- + \overline{K^0}$	1.0×10^{-6}	0.66	9.8×10^{-7}	0.41
$B^+ \rightarrow \rho^+ + K^0$	1.0×10^{-6} (9.4×10^{-7})		9.7×10^{-7} (8.9×10^{-7})	

Table 4:

$B \rightarrow PV$ ($b \rightarrow d$ transitions)				
Matrix Elements <i>with (without)</i> Strong Phases for $k^2 = m_b^2/2$				
CKM Matrix:	$\rho = 0.32, \eta = 0.31$		$\rho = -0.41, \eta = 0.18$	
Channel	BR	$a_{CP}[\%]$	BR	$a_{CP}[\%]$
$B^- \rightarrow \rho^- + \eta$	7.8×10^{-6}	6.5	1.8×10^{-5}	1.6
$B^+ \rightarrow \rho^+ + \eta$	6.8×10^{-6} (7.3×10^{-6})		1.7×10^{-5} (1.8×10^{-5})	
$B^- \rightarrow \rho^- + \eta'$	9.6×10^{-6}	14.	5.7×10^{-5}	1.2
$B^+ \rightarrow \rho^+ + \eta'$	7.2×10^{-6} (8.2×10^{-6})		5.6×10^{-5} (5.6×10^{-5})	
$B^- \rightarrow \rho^- + \pi^0$	2.3×10^{-5}	-2.0	1.7×10^{-5}	-1.5
$B^+ \rightarrow \rho^+ + \pi^0$	2.4×10^{-5} (2.3×10^{-5})		1.8×10^{-5} (1.8×10^{-5})	
$B^- \rightarrow \pi^- + J/\psi$	4.3×10^{-5} (4.3×10^{-5})	0.0	3.7×10^{-5} (3.7×10^{-5})	0.0
$B^- \rightarrow D^{*-} + D^0$	5.0×10^{-4}	0.89	4.7×10^{-4}	0.55
$B^+ \rightarrow D^{*+} + \overline{D^0}$	4.9×10^{-4} (5.0×10^{-4})		4.7×10^{-4} (4.7×10^{-4})	
$B^- \rightarrow \pi^- + \omega$	1.4×10^{-6}	-15.	1.3×10^{-6}	-9.7
$B^+ \rightarrow \pi^+ + \omega$	1.8×10^{-6} (1.6×10^{-6})		1.6×10^{-6} (1.4×10^{-6})	
$B^- \rightarrow \pi^- + \rho^0$	1.3×10^{-6}	11.	2.9×10^{-6}	2.5
$B^+ \rightarrow \pi^+ + \rho^0$	1.0×10^{-6} (1.2×10^{-6})		2.8×10^{-6} (2.9×10^{-6})	
$B^- \rightarrow \rho^- + \eta_c$	2.7×10^{-5} (2.7×10^{-5})	0.0	2.4×10^{-5} (2.4×10^{-5})	0.0
$B^- \rightarrow D^- + D^{0*}$	2.2×10^{-4}	0.23	2.2×10^{-4}	0.14
$B^+ \rightarrow D^+ + \overline{D^{0*}}$	2.2×10^{-4} (2.2×10^{-4})		2.2×10^{-4} (2.2×10^{-4})	
$B^- \rightarrow \pi^- + \phi$	1.1×10^{-7} (1.1×10^{-7})	0.0	4.0×10^{-7} (4.0×10^{-7})	0.0
$B^- \rightarrow K^{*-} + K^0$	3.5×10^{-8}	-21.	1.2×10^{-7}	-4.3
$B^+ \rightarrow K^{*+} + \overline{K^0}$	5.4×10^{-8} (4.2×10^{-8})		1.3×10^{-7} (1.1×10^{-7})	
$B^- \rightarrow K^- + K^{0*}$	4.7×10^{-7}	-18.	1.6×10^{-6}	-3.5
$B^+ \rightarrow K^+ + \overline{K^{0*}}$	6.7×10^{-7} (5.5×10^{-7})		1.7×10^{-6} (1.5×10^{-6})	

Table 5:

P_1	P_2	$Z_1^{(q)}$	$Z_2^{(q)}$
K^-	π^0	$(a_2\delta_{qu} + a_4 + a_6 R[K^-, \pi^0])/\sqrt{2}$	$a_1\delta_{qu}/\sqrt{2}$
K^-	η_u	$(a_2\delta_{qu} + a_4 + a_6 R[K^-, \eta_u])/\sqrt{2}$	$(a_1\delta_{qu} + 2a_3 + 2a_5)/\sqrt{2}$
K^0	π^-	$a_4 + a_6 R[K^0, \pi^-]$	0
K^-	η_s	0	$a_3 + a_4 + a_5 + a_6 R[\eta_s, K^-]$
D_s^-	D^0	0	$a_2\delta_{qc} + a_4 + a_6 R[D_s^-, D^0]$
K^-	η_c	0	$a_1\delta_{qc} + a_3 + a_5$
π^-	π^0	$(a_2\delta_{qu} + a_4 + a_6 R[\pi^-, \pi^0])/\sqrt{2}$	$(a_1\delta_{qu} - a_4 - a_6 R[\pi^0, \pi^-])/\sqrt{2}$
π^-	η_u	$(a_2\delta_{qu} + a_4 + a_6 R[\pi^-, \eta_u])/\sqrt{2}$	$(a_1\delta_{qu} + 2a_3 + a_4 + 2a_5 + a_6 R[\eta_u, \pi^-])/\sqrt{2}$
K^0	K^-	$a_4 + a_6 R[K^0, K^-]$	0
π^-	η_s	0	$a_3 + a_5$
D^-	D^0	0	$a_2\delta_{qc} + a_4 + a_6 R[D^-, D^0]$
π^-	η_c	0	$a_1\delta_{qc} + a_3 + a_5$

This figure "fig1-1.png" is available in "png" format from:

<http://arxiv.org/ps/hep-ph/9410406v2>

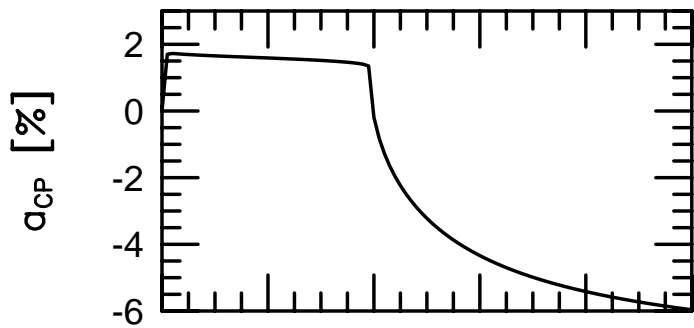
This figure "fig2-1.png" is available in "png" format from:

<http://arxiv.org/ps/hep-ph/9410406v2>

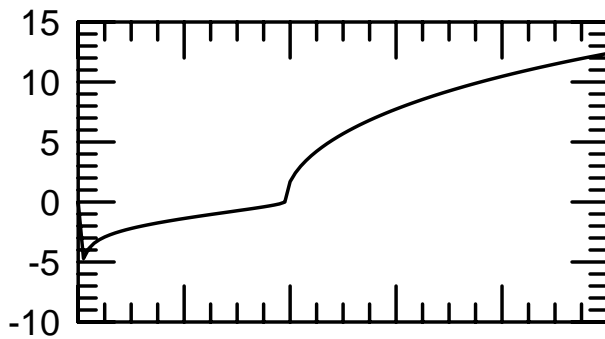
This figure "fig2-2.png" is available in "png" format from:

<http://arxiv.org/ps/hep-ph/9410406v2>

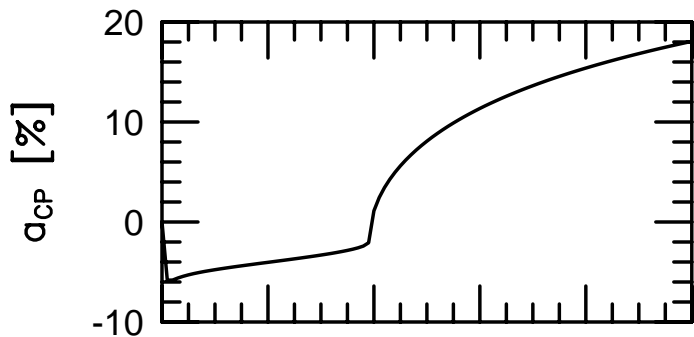
$B \rightarrow K^- \eta$



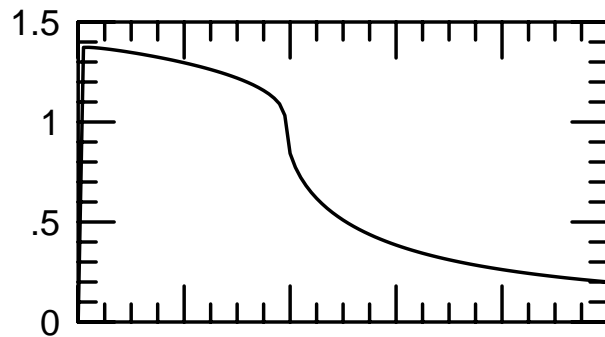
$B \rightarrow K^- \eta'$



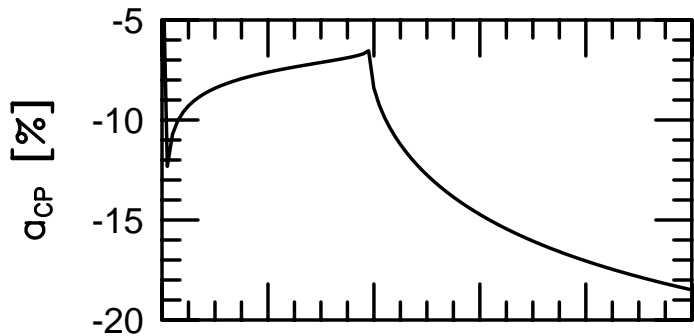
$B \rightarrow K^- \pi^0$



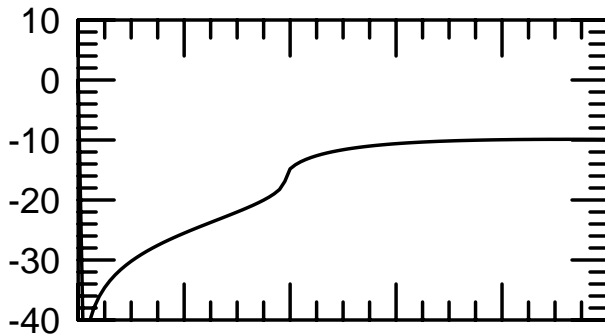
$B \rightarrow \pi^- K^0$



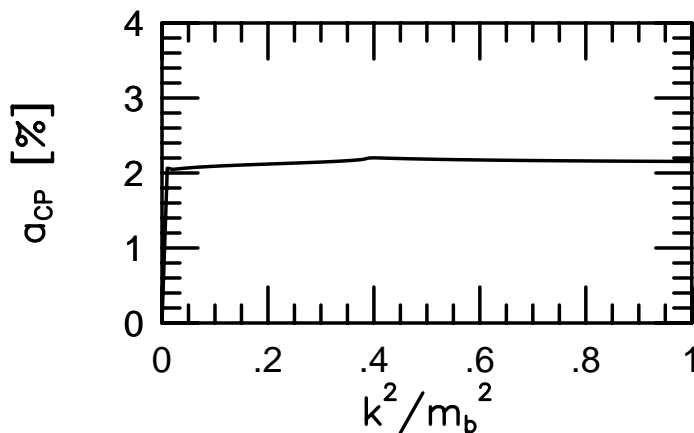
$B \rightarrow \pi^- \eta$



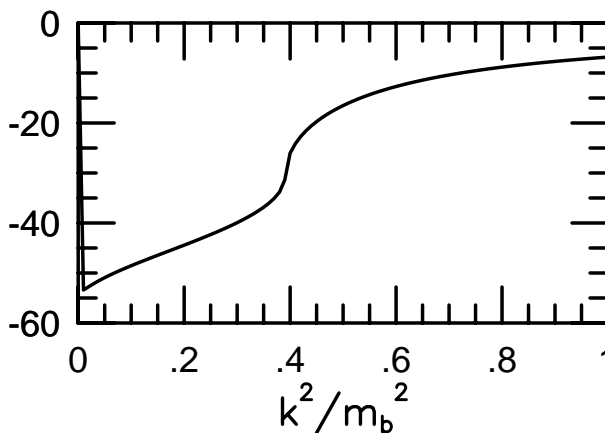
$B \rightarrow \pi^- \eta'$



$B \rightarrow D^- D^0$



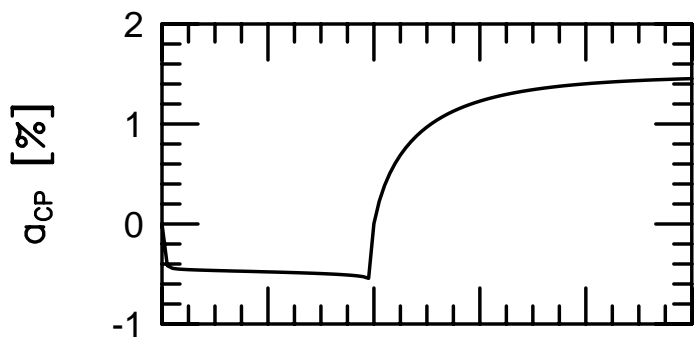
$B \rightarrow K^- K^0$



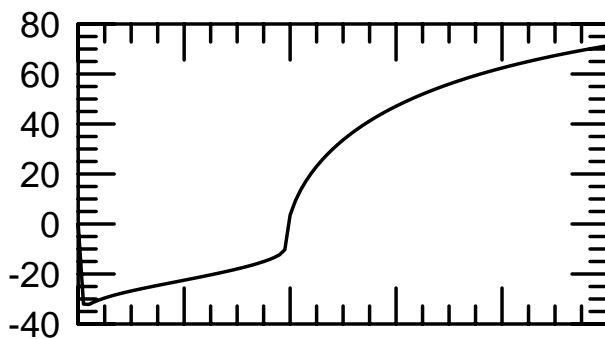
This figure "fig2-3.png" is available in "png" format from:

<http://arxiv.org/ps/hep-ph/9410406v2>

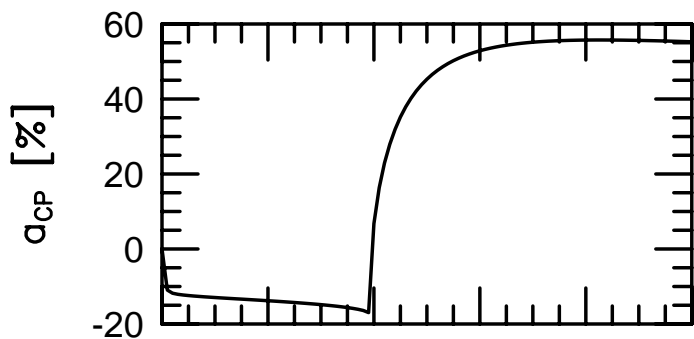
$B \rightarrow K^- \omega$



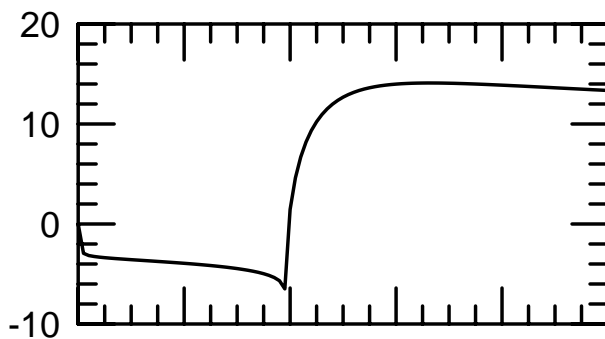
$B \rightarrow K^- \rho^0$



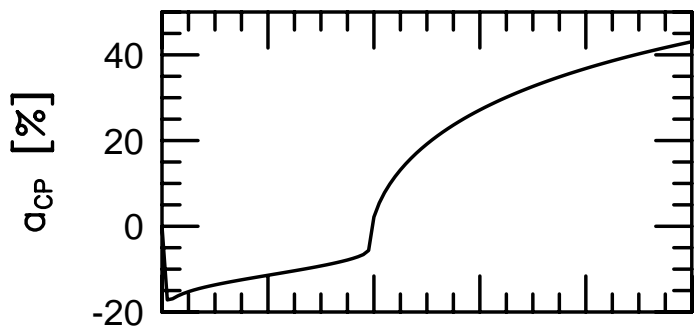
$B \rightarrow K^{*-} \eta$



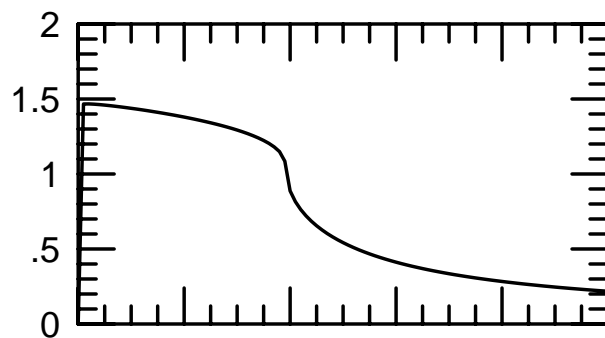
$B \rightarrow K^{*-} \eta'$



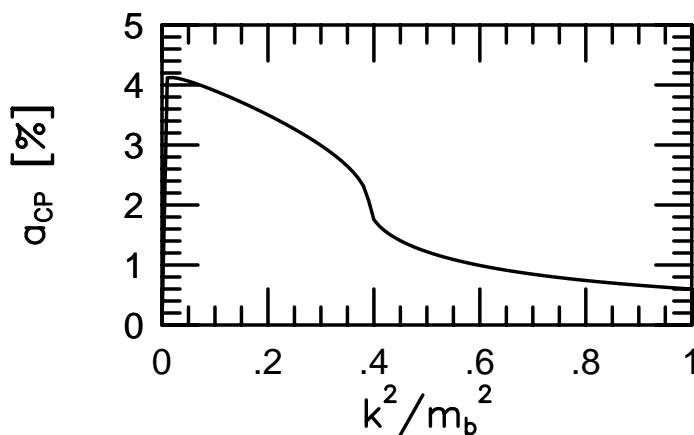
$B \rightarrow K^{*-} \pi^0$



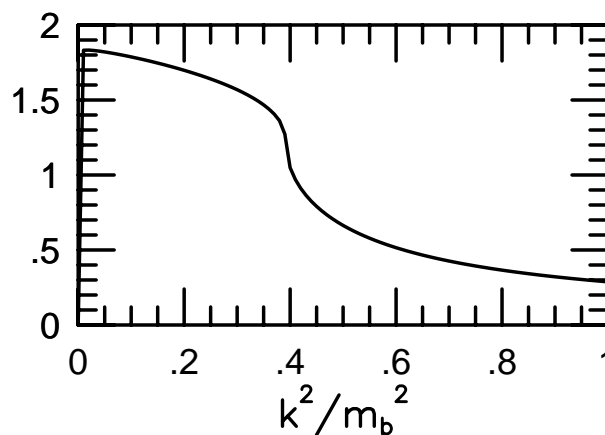
$B \rightarrow \pi^- K^{*0}$



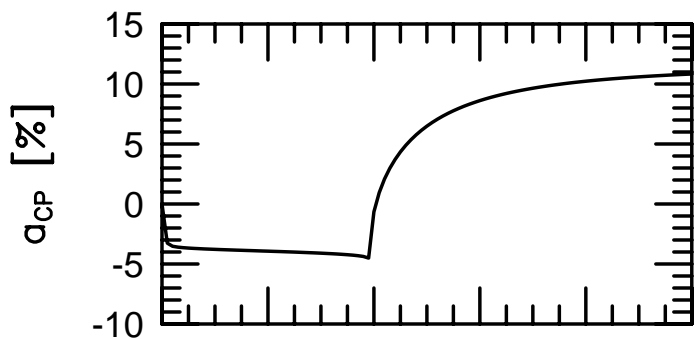
$B \rightarrow K^- \phi$



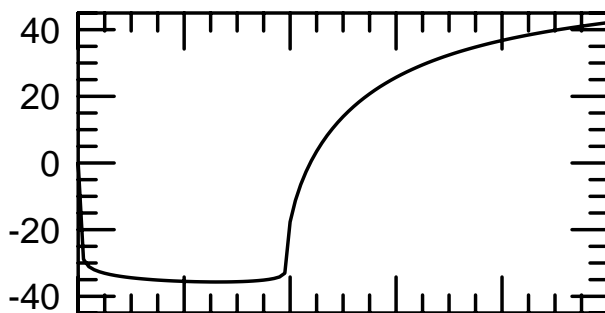
$B \rightarrow \rho^- K^0$



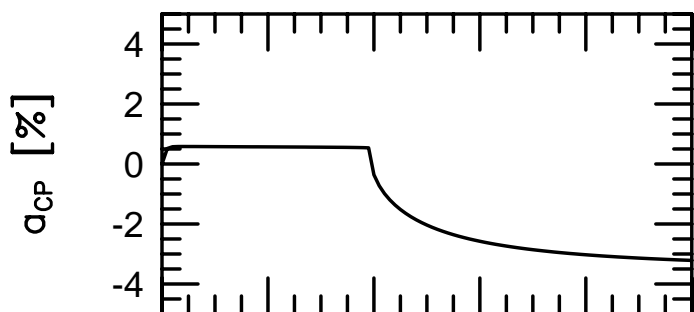
$B \rightarrow \rho^- \eta$



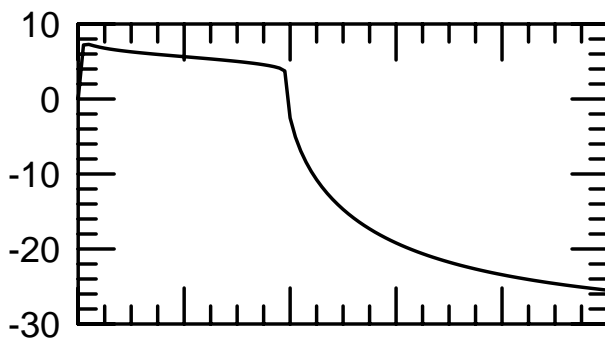
$B \rightarrow \rho^- \eta'$



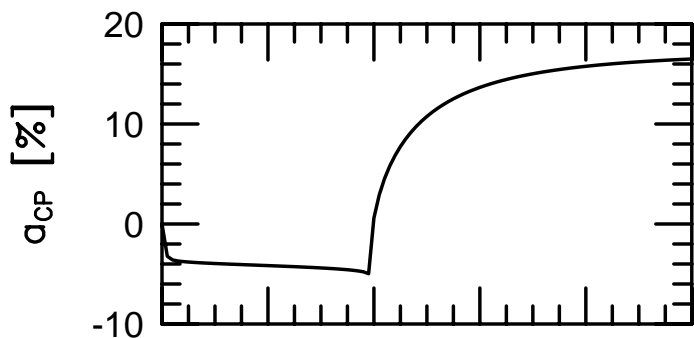
$B \rightarrow \rho^- \pi^0$



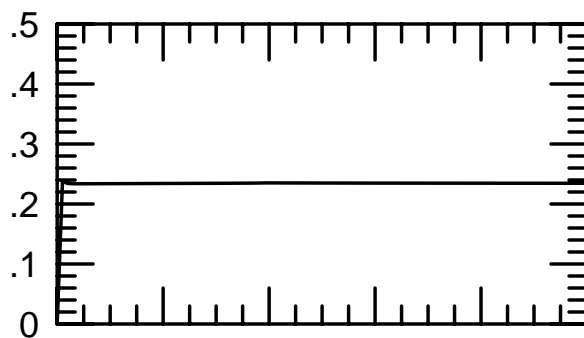
$B \rightarrow \pi^- \omega$



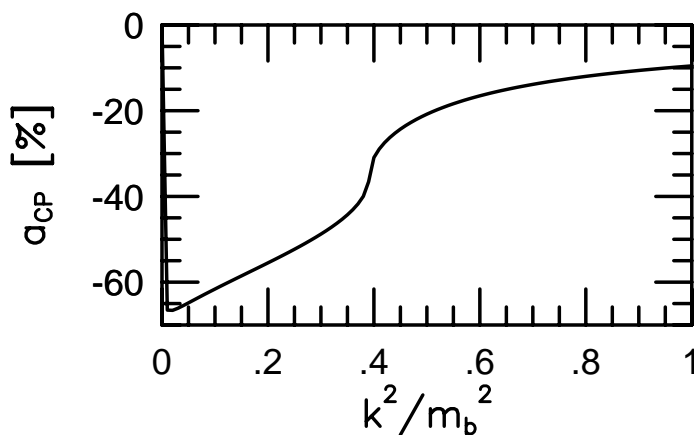
$B \rightarrow \pi^- \rho^0$



$B \rightarrow D^- D^{*0}$



$B \rightarrow K^{*-} K^0$



$B \rightarrow K^- K^{*0}$

